Effect of Axial Diffusion of Vorticity on Flow Development in Circular Conduits: Part I. Numerical Solutions

J. S. VRENTAS, J. L. DUDA, and K. G. BARGERON

Dow Chemical Company, Midland, Michigan

An entrance model is presented which extends the analysis of the flow development in the entrance region to flow regimes which are inadequately described by a boundary-layer analysis. Results are presented for the numerical solutions of the boundary-layer equations and the complete equations of motion at five different Reynolds numbers. The effect of the axial diffusion of vorticity on the pressure drop, entrance length, and development of the vorticity and velocity fields is demonstrated.

Since the pioneering work of Prandtl early in this century, boundary-layer theory has provided the principal basis for the theoretical analysis of laminar flow phenomena near solid boundaries. It is now possible to conduct a more rigorous analysis of laminar flows, since the development of high-speed computers and sophisticated numerical techniques permit the solution of the complete set of field equations describing a particular fluid motion. In this paper, the development of the steady, laminar flow of an incompressible Newtonian fluid in the entrance of a circular tube is analyzed by the numerical solution of both the boundary-layer equations and the complete equations of motion.

In both the theoretical analysis and the qualitative description of this flow situation, it is useful to consider the development of the corresponding vorticity field. [An excellent discussion of vorticity and its relation to the development of fluid flows has been presented by Lighthill (9)]. In an idealized entrance, fluid initially free of vorticity develops a vorticity field as it enters the conduit. The vorticity, which is imparted to the fluid, is continuously generated at the solid surface of the tube in just the amount required to maintain the nonslip condition of the tangential velocity. This vorticity is then transported from the conduit wall by convective and diffusive flows. In boundary-layer theory the axial diffusion of vorticity and all terms of the same order of magnitude are assumed to have negligible effect on the development of flow.

In previous studies which employed the boundary-layer equations, it has been assumed that a uniform velocity profile exists at the entrance of the tube. However, when the complete equations of motion, including terms which describe the axial diffusion of vorticity, are solved, the boundary conditions in the region preceding the tube entrance must be specified. This is due to the fact that under certain conditions the developing velocity field in the entrance section of the tube will significantly influence the velocity field in the upstream region. The entrance model considered in this analysis has been defined so that the velocity profile at the entrance reduces to the plug flow case when the boundary-layer assumptions are imposed. It should be noted that the entrance configuration used here is the only entrance model which will predict exactly a uniform velocity profile at the tube entrance when axial diffusion of vorticity is neglected. Therefore, this model permits a direct extension of the previous boundary-layer studies.

In the proposed model, the region upstream from the entrance is considered to be a stream tube of the same diameter as the tubular conduit. This stream tube is assumed to be impermeable, frictionless, and infinite in extent. Since the fluid in the stream tube far upstream from the pipe entrance is considered void of vorticity, this model presents a very sensitive test of the effect of the axial diffusion of vorticity on the velocity profile development, because the only solid surface which is available for the generation of vorticity is the wall of the conduit. There exist no solid surfaces upstream to complicate the vorticity field. To complete the model, the circular conduit is considered to be infinite in extent with a fully developed parabolic velocity profile existing far downstream from the entrance.

This entrance model will be exact only for the unusual physical situation in which the tube is placed in a flowing stream with the particular property that the resistance to flow is the same for the fluid entering and bypassing the tube. Such a flow situation is difficult to realize exactly physically. However, the results that follow show that the analysis based on this model should be a good approximation for any entrance configuration which attempts to produce plug flow at the entrance. This is so because the effective length of the stream tube proves to be less than one tube diameter. In other words, the effects of the axial diffusion of vorticity are significant only in a very short region upstream from the entrance of the conduit. Preliminary considerations neglecting axial vorticity transport by diffusion indicate that most entrance configurations should produce approximately uniform velocity profiles at the tube entrance. One familiar example is the flow from a large reservoir through a well-rounded entrance duct. Even though the axial diffusion of vorticity from the tube wall will not permit the existence of a uniform profile right at the entrance, the fluid, a very short distance upstream, will be out of the influence of this vorticity and should closely approach uniform flow. Hence, the entrance model analyzed in this study should give a reasonable approximation to the upstream flow field in the region immediately adjacent to the tube entrance.

In this study we could have taken the alternative approach of analyzing an exact representation of a specific experimental entrance configuration. However, most such entrances involve complex upstream geometries which are difficult to describe mathematically and which greatly

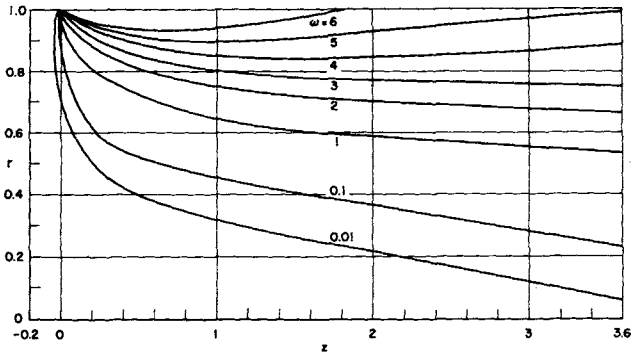

Fig. 1. Vorticity distribution, $N_{Re} = 250$.

complicate the numerical solution. In addition, each such solution would be specific and would offer limited information toward a general understanding of flow development in tubes. Like its precursors, which are the boundary-layer solutions of entrance flow with initial uniform velocity profiles, this study is an attempt to describe a flow situation which can be considered a good approximation to many specific cases. However, extensive experimental data in the Reynolds number range in which the results of this study deviate from a boundary-layer analysis are needed before the applicability of this entrance model to a variety of real systems can be completely justified.

It should be noted that a similar stream tube model has been used by Wang and Longwell (*13*) in their analysis of flow development between parallel plates at a Reynolds number of 300. This model is exact for the case of an infinite set of parallel plates submerged in a fluid of uniform motion. Another example of a numerical solution of the elliptic equations of motion for a different physical situation is the recent work of Paris and Whitaker (*11*).

Although the axial diffusion of vorticity is effective only for a small distance upstream, very significant changes in the velocity profile can occur in this region. Solution of the complete set of field equations for this stream tube model extends the analysis of flow development in tubes to flow regimes which are inadequately described by a boundary-layer analysis. In addition, a comparison of the numerical solutions of the complete set of field equations and the boundary-layer equations indicates the conditions under which the boundary-layer assumptions can be considered valid.

DEVELOPMENT OF EQUATIONS

For the entrance configuration described above we consider the isothermal, steady state, laminar flow of an incompressible Newtonian fluid with constant viscosity. The analysis is further restricted either to any pipe with gravity neglected or to a vertical pipe with the body force term incorporated into the pressure gradient (*1*). These restrictions make it possible to assume symmetry in the azimuthal direction and to set the velocity in this direction everywhere equal to zero. Consequently, the dimensionless forms of the equations of motion and the continuity equation become

$$V\frac{\partial V}{\partial r} + U\frac{\partial V}{\partial z} = -\frac{1}{U_a{}^2\rho}\frac{\partial p}{\partial r} + \frac{2}{N_{Re}}\left(\frac{\partial^2 V}{\partial r^2} + \frac{1}{r}\frac{\partial V}{\partial r} - \frac{V}{r^2} + \frac{\partial^2 V}{\partial z^2}\right) \quad (1)$$

$$V\frac{\partial U}{\partial r} + U\frac{\partial U}{\partial z} = -\frac{1}{U_a{}^2\rho}\frac{\partial p}{\partial z} + \frac{2}{N_{Re}}\left(\frac{\partial^2 U}{\partial r^2} + \frac{1}{r}\frac{\partial U}{\partial r} + \frac{\partial^2 U}{\partial z^2}\right) \quad (2)$$

$$\frac{\partial V}{\partial r} + \frac{V}{r} + \frac{\partial U}{\partial z} = 0 \quad (3)$$

Since it proves to be more convenient to work in terms of a stream function and a vorticity, the dimensionless stream function ψ is introduced in the usual manner:

$$U = -\frac{1}{r}\frac{\partial \psi}{\partial r} \quad (4)$$

$$V = \frac{1}{r}\frac{\partial \psi}{\partial z} \quad (5)$$

It is evident from Equations (4) and (5) that the stream function satisfies the dimensionless continuity equation identically. Furthermore, for this flow field, the only nonzero component of the vorticity vector (*12*)

$$\omega^i = \frac{e^{ijk}}{\sqrt{g}} v_{k,j} \quad (6)$$

is the azimuthal physical component

$$\omega = \frac{\partial V}{\partial z} - \frac{\partial U}{\partial r} \quad (7)$$

Differentiation of Equation (1) with respect to z, differentiation of Equation (2) with respect to r, subtraction of the resultant two equations, substitution of Equations (4), (5), and (7), and utilization of the continuity equation give

$$-\frac{\omega}{r^2}\frac{\partial \psi}{\partial z} + \frac{1}{r}\frac{\partial \psi}{\partial z}\frac{\partial \omega}{\partial r} - \frac{1}{r}\frac{\partial \psi}{\partial r}\frac{\partial \omega}{\partial z} = \frac{2}{N_{Re}}\left(\frac{\partial^2 \omega}{\partial r^2} + \frac{1}{r}\frac{\partial \omega}{\partial r} - \frac{\omega}{r^2} + \frac{\partial^2 \omega}{\partial z^2}\right) \quad (8)$$

A more general derivation of Equation (8), usually referred to as the vorticity transport equation, is given in the Appendix. The terms on the left-hand side of this equation represent convective flow of the azimuthal component of the vorticity vector and vorticity generation due to the deformation of vortex tubes, whereas those on the right-hand side describe the radial and axial diffusion of this vorticity component. Substitution of Equations (4) and (5) into Equation (7) gives the necessary additional relationship between the vorticity and the stream function:

$$\omega r = \frac{\partial^2 \psi}{\partial z^2} + \frac{\partial^2 \psi}{\partial r^2} - \frac{1}{r}\frac{\partial \psi}{\partial r} \quad (9)$$

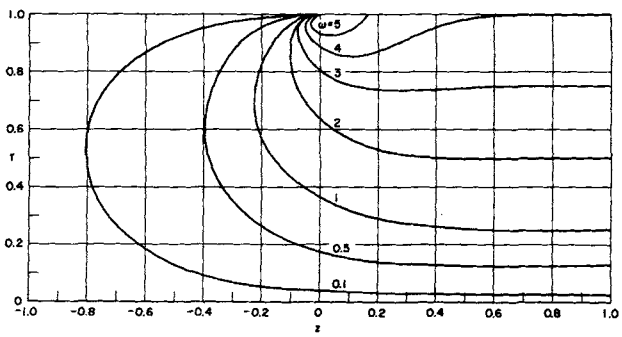

Fig. 2. Vorticity distribution, $N_{Re} = 1$.

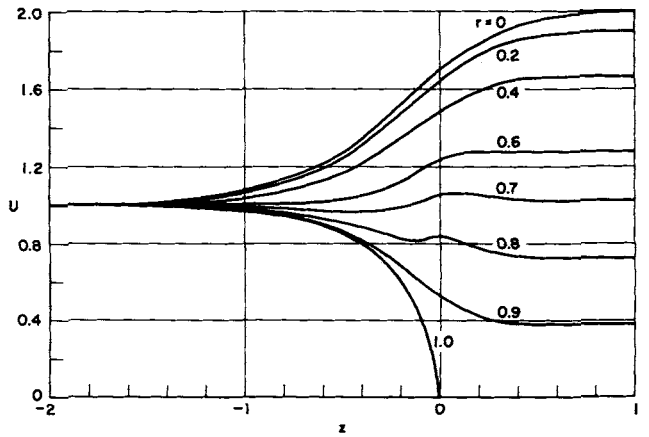

Fig. 3. Velocity distribution, $N_{Re} = 0$, $k_r = 3.0$, $k_s = 0.75$.

For the infinite region composed of the stream tube and the real tube, the following boundary conditions are applicable:

$$U = V = \psi = (\partial\psi/\partial r) = 0 \text{ for } r = 1,\ z > 0 \quad (10)$$

$$(\partial U/\partial r) = V = \omega = 0,\ \psi = 1/2 \text{ for } r = 0,\ -\infty < z < \infty \quad (11)$$

$$(\partial U/\partial r) = V = \omega = \psi = 0 \text{ for } r = 1,\ z < 0 \quad (12)$$

$$V = \omega = 0,\ U = 1,\ \psi = 1/2\,(1 - r^2) \text{ for } z = -\infty,\quad 0 \leqq r \leqq 1 \quad (13)$$

$$V = 0,\ U = 2\,(1 - r^2),\ \omega = 4r,$$

$$\psi = r^2\,(r^2/2 - 1) + 1/2 \text{ for } z = +\infty,\ 0 \leqq r \leqq 1 \quad (14)$$

Equation (12) illustrates the absence of any generation of vorticity at the impermeable stream tube wall due to the zero shear stress at this surface.

Solution of Equations (8) and (9) with boundary conditions given by Equations (10) to (14) leads to a complete description of the velocity and pressure fields for the system under consideration. However, there arise two principal difficulties in the derivation of the desired solution. First, there is the absence of a boundary condition for the vorticity at the real tube wall. It is known (*10*) that a unique, stable solution exists for a single elliptic partial differential equation if the region under consideration has a closed boundary with Dirichlet or Neumann boundary conditions specified over the entire boundary. It is assumed that this criterion can be extended to the two coupled elliptic equations being considered here. From the above boundary conditions, it is evident that the uniqueness requirement is satisfied on all boundaries, except the real tube wall where there exists a Cauchy condition for the stream function but no boundary condition for the vorticity. However, it is possible to generate the following condition for the vorticity at the real tube wall by evaluating Equation (9) at $r = 1$ and utilizing Equation (10):

$$\omega = (\partial^2\psi/\partial r^2) \quad (15)$$

This equation guarantees that the normal derivative of the stream function vanishes at $r = 1$ and, in addition, provides a boundary condition for the vorticity in terms of the radial stream function distribution in the tube. Consequently, Equation (15) and the vanishing of the stream function are considered to be the proper boundary conditions at the wall of the real tube.

The second difficulty arises because the region under consideration is infinite in extent in the z direction. Since Equation (8) is nonlinear, the stream function and vorticity equations must be solved numerically; in practice, it is not possible in the strictest sense to solve an elliptic equation for an infinite region with a closed boundary by a numerical method. To circumvent this difficulty, the infinite region $z = -\infty$ to $z = +\infty$ is mapped into the finite region $\eta = -1$ to $\eta = +1$ by application of the following coordinate transformation:

$$\eta = \tanh kz \quad (16)$$

This particular transformation is useful because it can be chosen to be continuous throughout the entire region if desired, and because it permits (by proper choice of the parameter k) the amplification of the region near $z = 0$, which is the region of greatest importance for this flow situation. Substitution of Equation (16) into Equations (8) and (9) yields the following elliptic differential equations:

$$k(1-\eta^2)\left[-\frac{\omega}{r^2}\frac{\partial\psi}{\partial\eta} + \frac{1}{r}\frac{\partial\psi}{\partial\eta}\frac{\partial\omega}{\partial r} - \frac{1}{r}\frac{\partial\psi}{\partial r}\frac{\partial\omega}{\partial\eta}\right] = \frac{2}{N_{Re}}\left[\frac{\partial^2\omega}{\partial r^2} + \frac{1}{r}\frac{\partial\omega}{\partial r} - \frac{\omega}{r^2} + (1-\eta^2)^2 k^2\left(\frac{\partial^2\omega}{\partial\eta^2}\right) - 2k^2\eta(1-\eta^2)\frac{\partial\omega}{\partial\eta}\right] \quad (17)$$

$$r\omega = (1-\eta^2)^2 k^2\left(\frac{\partial^2\psi}{\partial\eta^2}\right) + \frac{\partial^2\psi}{\partial r^2} - 2k^2\eta(1-\eta^2)\frac{\partial\psi}{\partial\eta} - \frac{1}{r}\frac{\partial\psi}{\partial r} \quad (18)$$

Equations for Negligible Axial Diffusion of Vorticity

At high Reynolds numbers where the convective transport of vorticity in the axial direction overwhelms the axial diffusive transport, a standard order of magnitude analysis shows that the axial diffusion term in the vorticity transport equation is much smaller than each of the other terms. Furthermore, the $(\partial^2\psi/\partial z^2)$ term in Equation (9) is negligible in comparison with the other terms of this equation. Consequently, at high Reynolds numbers Equations (8) and (9) reduce to

$$-\frac{\omega}{r^2}\frac{\partial\psi}{\partial z} + \frac{1}{r}\frac{\partial\psi}{\partial z}\frac{\partial\omega}{\partial r} - \frac{1}{r}\frac{\partial\psi}{\partial r}\frac{\partial\omega}{\partial z} = \frac{2}{N_{Re}}\left[\frac{\partial^2\omega}{\partial r^2} + \frac{1}{r}\frac{\partial\omega}{\partial r} - \frac{\omega}{r^2}\right] \quad (19)$$

$$\omega r = \frac{\partial^2\psi}{\partial r^2} - \frac{1}{r}\frac{\partial\psi}{\partial r} \quad (20)$$

These equations can also be derived by first applying the usual boundary-layer arguments (*7*) to Equations (1), (2), and (3) and then by employing a definition of the vorticity modified by order of magnitude considerations. Equations (19) and (20) are second-order, parabolic differential equations. It is known (*10*) that a unique, stable solution exists for a single parabolic partial differential equation if Dirichlet or Neumann conditions are specified on an open boundary. The unspecified part of the boundary must be at the positive infinite limit of the independent time variable (in this case, z). Once again this requirement is met for the two coupled equations of interest everywhere but on the real tube wall. This difficulty is resolved in the manner described above. Consequently, Equations (10), (11), (12), (13), and (15) are the necessary conditions specified on an open boundary of the infinite region composed of the stream tube and the real tube.

If Equations (19) and (20) are solved subject to Equations (11), (12), and (13) for the region $z < 0$, $0 \leqq r \leqq 1$, there results

$$\omega = 0 \quad (21)$$

$$\psi = \frac{1}{2}(1 - r^2) \tag{22}$$

$$U = 1 \tag{23}$$

for all z in the stream tube. It is evident that with no axial diffusion of vorticity the flow field in the stream tube is not influenced by the flow development in the real tube; the velocity profile remains undisturbed until it reaches the real tube entrance. The problem then reduces to solving Equations (19) and (20) subject to Equations (10), (11), (15), (21), and (22) for the region $z \geqq 0$, $0 \leqq r \leqq 1$. Consequently, in the limit of high Reynolds numbers where the axial diffusion of vorticity becomes vanishingly small, the entrance model proposed above reduces to the familiar entrance flow model with the boundary-layer equations describing the flow development and with a uniform profile at the tube entrance.

Finally, it is convenient for numerical calculations to eliminate the Reynolds number from Equation (19). Substitution of the new independent variable

$$\zeta = \frac{2z}{N_{Re}} \tag{24}$$

into Equation (19) yields

$$-\frac{\omega}{r^2}\frac{\partial\psi}{\partial\zeta} + \frac{1}{r}\frac{\partial\psi}{\partial\zeta}\frac{\partial\omega}{\partial r} - \frac{1}{r}\frac{\partial\psi}{\partial r}\frac{\partial\omega}{\partial\zeta} = \frac{\partial^2\omega}{\partial r^2} + \frac{1}{r}\frac{\partial\omega}{\partial r} - \frac{\omega}{r^2} \tag{25}$$

NUMERICAL METHODS OF SOLUTION

Elliptic Finite-Difference Equations

Because of the azimuthal symmetry of the infinite cylinder comprising the flow field, it is possible to utilize a rectangular grid composed of the region $0 \leqq r \leqq 1$, $-1 \leqq \eta \leqq 1$ in deriving the finite-difference representation of the basic equations. The radial subscript i takes on integer values between 0 and N and the axial subscript j assumes integer values between $-M$ and M. Introduction of the standard central difference approximations to first and second derivatives (3) into Equations (18) and (17) gives the following two elliptic finite-difference equations for every interior point (i, j) of the finite-difference network:

$$AS\,\psi_{i-1,j} + BS\,\psi_{i,j} + CS\,\psi_{i+1,j} = DS\,\psi_{i,j-1} + ES\,\psi_{i,j+1} + FS\,\omega_{i,j} \tag{26}$$

$$AW\,\omega_{i,j-1} + BW\,\omega_{i,j} + CW\,\omega_{i,j+1} = DW\,\omega_{i-1,j} + EW\,\omega_{i+1,j} \tag{27}$$

$$AS = 1 + 1/2i \tag{28}$$

$$BS = -2k^2\left(\frac{\Delta r}{\Delta\eta}\right)^2[1 - j^2(\Delta\eta)^2]^2 - 2 \tag{29}$$

$$CS = 1 - 1/2i \tag{30}$$

$$DS = -k^2\left(\frac{\Delta r}{\Delta\eta}\right)^2[1 - j^2(\Delta\eta)^2]^2 - jk^2(\Delta r)^2[1 - j^2(\Delta\eta)^2] \tag{31}$$

$$ES = -k^2\left(\frac{\Delta r}{\Delta\eta}\right)^2[1 - j^2(\Delta\eta)^2]^2 + jk^2(\Delta r)^2[1 - j^2(\Delta\eta)^2] \tag{32}$$

$$FS = i(\Delta r)^3 \tag{33}$$

$$AW = k[1 - j^2(\Delta\eta)^2]\left\{\frac{\psi_{i+1,j} - \psi_{i-1,j}}{4i(\Delta\eta)(\Delta r)^2} - \frac{2k[1 - j^2(\Delta\eta)^2]}{N_{Re}(\Delta\eta)^2} - \frac{2kj}{N_{Re}}\right\} \tag{34}$$

$$BW = -\frac{k[1 - j^2(\Delta\eta)^2]}{2i^2(\Delta\eta)(\Delta r)^2}(\psi_{i,j+1} - \psi_{i,j-1}) + \frac{4}{N_{Re}(\Delta r)^2} + \frac{2}{N_{Re}\,i^2(\Delta r)^2} + \frac{4k^2[1 - j^2(\Delta\eta)^2]^2}{N_{Re}(\Delta\eta)^2} \tag{35}$$

$$CW = -k[1 - j^2(\Delta\eta)^2]\left\{\frac{\psi_{i+1,j} - \psi_{i-1,j}}{4i(\Delta\eta)(\Delta r)^2} - \frac{2kj}{N_{Re}} + \frac{2k}{N_{Re}(\Delta\eta)^2}[1 - j^2(\Delta\eta)^2]\right\} \tag{36}$$

$$DW = \frac{k[1 - j^2(\Delta\eta)^2]}{4i(\Delta\eta)(\Delta r)^2}(\psi_{i,j+1} - \psi_{i,j-1}) + \frac{2}{N_{Re}(\Delta r)^2}(1 - 1/2i) \tag{37}$$

$$EW = -\frac{k[1 - j^2(\Delta\eta)^2]}{4i(\Delta\eta)(\Delta r)^2}(\psi_{i,j+1} - \psi_{i,j-1}) + \frac{2}{N_{Re}(\Delta r)^2}(1 + 1/2i) \tag{38}$$

In order to obtain accurate numerical solutions, it is necessary to expand the stream tube differently than the real tube by introducing two different values of the amplification parameter k into the numerical scheme. Hence, for interior points with $j > 0$, the parameter k in Equations (26) to (38) is replaced by k_r, the real tube expansion factor, and for interior points with $j < 0$ a stream tube expansion factor k_s must be used. In addition, the coefficients of Equations (26) and (27) must be modified for the interior grid points at $j = 0$ because of the discontinuous derivatives with respect to the variable η at that coordinate surface. Finite-difference equations were derived for the grid points at $j = 0$ by utilizing standard Taylor series techniques and by requiring that the first, second, and third derivatives of the field variables with respect to z be continuous at $\eta = 0$.

A successive implicit line iteration method (5) was used to obtain the solution to Equations (26) and (27). For this method, values of the approximate solution are improved simultaneously on an entire line of grid points; furthermore, improved values are used as soon as they are available. At each value of j in the η direction, $N - 1$ equations of the form of Equation (26), one for each grid point, can be consolidated into a matrix equation which can be solved by tridiagonal matrix inversion (3) to give new values of the stream function at that grid line. Similarly, at each value of i in the r direction, the $2M - 1$ equations of the form of Equation (27) yield a matrix equation with a tridiagonal coefficient matrix. Again, a simple Gaussian elimination procedure facilitates inversion of the coefficient matrix, giving new values of the vorticity at the grid line of interest as the solution to

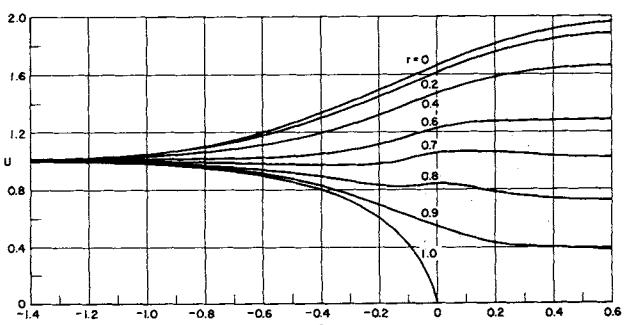

Fig. 4. Velocity distribution, $N_{Re} = 1$, $k_r = 1.2$, $k_s = 1.0$.

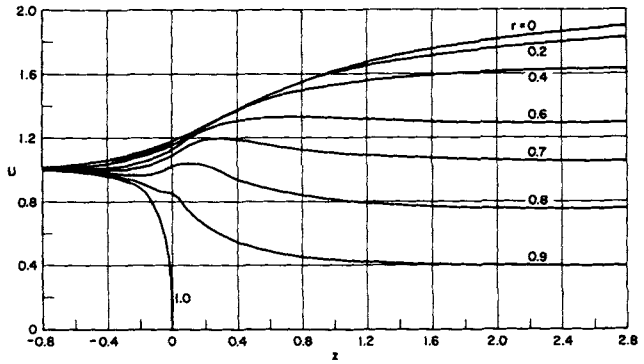

Fig. 5. Velocity distribution, $N_{Re} = 50$, $k_r = 0.6$, $k_s = 6.0$.

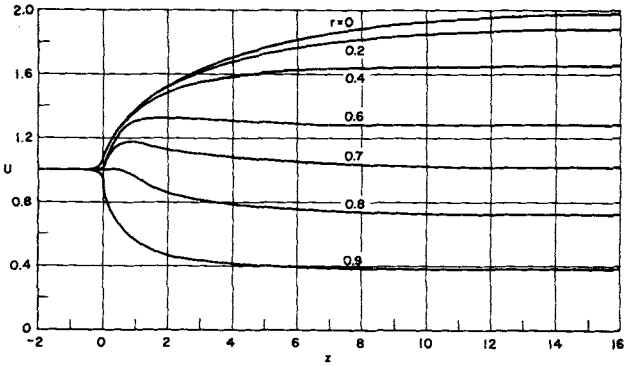

Fig. 6. Velocity distribution, $N_{Re} = 150$, $k_r = 0.14$, $k_s = 15$.

the matrix equation. All of the boundary conditions enter trivially into the iterative solution with the exception of the condition for vorticity at the real tube wall. The following finite-difference form of Equation (15) was derived from a Taylor series expansion for the stream function:

$$\omega_{N,j} = \frac{4\psi_{N-1,j}}{(\Delta r)^2} - \frac{\psi_{N-2,j}}{2(\Delta r)^2} \tag{39}$$

The iterative method of numerical solution can be summarized as follows:

1. Assume initial values for ψ and ω throughout the interior of the region and for ω on the real tube wall.
2. Calculate new values of ψ for each of the $2M - 1$ grid lines perpendicular to the axial direction (for each value of j) by using a line-by-line matrix inversion technique with Equation (26).
3. Update the values of ω at the real tube wall by using Equation (39).
4. Calculate new values of ω for each of the $N - 1$ grid lines perpendicular to the radial direction (for each value of i) by using the line-by-line matrix inversion method with Equation (27).
5. Test ψ and ω to see if the convergence criteria are satisfied.
6. Repeat steps 2, 3, 4, and 5 if necessary.

Each iteration of this computational scheme takes the stream function and vorticity fields closer to the exact solution (subject to round off error) of the finite-difference equations. The finite-difference solution was considered converged when an additional iteration did not cause more than a 0.1% change in ψ and ω values at all grid points. The relative convergence of the two field variables was quite different, for when the vorticity field had reached this convergence of 0.1%, all values of the stream function had converged to a fractional error of several orders of magnitude smaller.

In the numerical solution the grid size in the transformed coordinate system is controlled by the values of N and M, and the distribution of the grid points in the z coordinate system is controlled by the parameters k_r and k_s. The accuracy which can be obtained with a given grid size can be improved by changing the values of k_r and k_s to obtain proper expansion of the transformed coordinate systems of the real and stream tubes near the tube entrance. For any given Reynolds number there exists a range of values for these expansion parameters which will give good accuracy. The values of the expansion parameters which were employed in the several cases analyzed are given in Figures 3 to 7. As the Reynolds number is decreased, the velocity development takes place over more of the stream tube region and the amplification factor k_s must subsequently be reduced. By similar reasoning, k_r must be decreased as the Reynolds number increases because of the greater amount of flow development in the real tube.

Poor choices for the values of k_r and k_s will not only affect the accuracy of the finite-difference approximation to the differential equations but can also lead to stability problems. However, in this study it was always possible to avoid completely any unstable behavior even at the higher Reynolds numbers by judicious choices for k_r and k_s.

The cases considered were first analyzed with a grid network with $N = 10$ and $M = 10$. Then, solutions were obtained on an expanded grid which was obtained by increasing N to a value of 20 and by changing the values of k_r and k_s to give a threefold increase in expansion in the axial direction near the tube entrance. The excellent agreement between the two solutions for all cases considered was considered a good indication that the finite-difference solution had converged to the solution of the original partial differential equations.

The excellent agreement between the numerical solution at $N_{Re} = 0$ and an analytical solution valid for very low Reynolds numbers gave further evidence that the local discretization error was everywhere small. Details of the analytical solution are given in a subsequent communication.

Once the vorticity and stream function arrays were repetitively iterated to the desired degree of accuracy, the radial and axial pressure gradients were computed from the finite-difference forms of Equations (1) and (2) (expressed in the $\eta - r$ coordinate frame), and the axial and radial velocities were calculated from the finite-difference approximations to Equation (4) and to

$$V = \frac{k(1-\eta^2)}{r}\frac{\partial\psi}{\partial\eta} \tag{40}$$

Total pressure drop was calculated by integrating the axial pressure gradient at a given radius.

Parabolic Finite-Difference Equations

For the parabolic differential equations, it is necessary to consider only the region $0 \leqq r \leqq 1$, $\zeta \geqq 0$. Hence, the radial subscript i in the finite-difference representation again assumes integer values between 0 and N, but the axial subscript j ranges from $j = 0$ to any value desired. Substitution of the usual central difference approximations for the radial derivatives and of a backward difference approximation for the first derivatives in the axial direction (3) into Equations (20) and (25) gives the following two parabolic finite-difference equations for every interior point $(i, j+1)$ of the finite-difference network:

$$(2i+1)\,\psi_{i-1,j+1} - 4i\,\psi_{i,j+1} + (2i-1)\,\psi_{i+1,j+1} = 2i^2(\Delta r)^3\,\omega_{i,j+1} \tag{41}$$

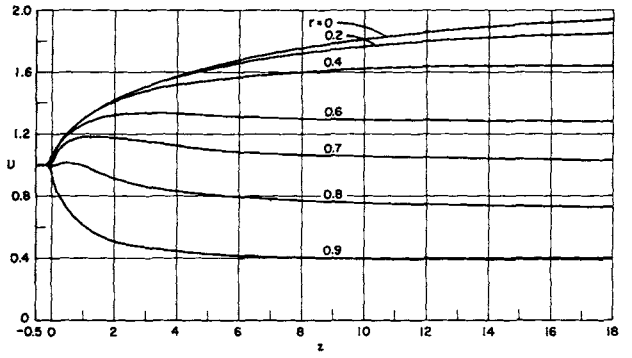

Fig. 7. Velocity distribution, $N_{Re} = 250$, $k_r = 0.10$, $k_s = 20$.

$$FW\,\omega_{i-1,j+1} + GW\,\omega_{i,j+1} + HW\,\omega_{i+1,j+1} = IW\,\omega_{i,j} \quad (42)$$

$$FW = 2i^2 - i + \frac{i}{\Delta\zeta}(\psi_{i,j+1} - \psi_{i,j}) \quad (43)$$

$$GW = -4i^2 - 2 + \frac{i}{\Delta\zeta}(\psi_{i+1,j+1} - \psi_{i-1,j+1}) + \frac{2(\psi_{i,j+1} - \psi_{i,j})}{\Delta\zeta} \quad (44)$$

$$HW = 2i^2 + i - \frac{i}{\Delta\zeta}(\psi_{i,j+1} - \psi_{i,j}) \quad (45)$$

$$IW = \frac{i}{\Delta\zeta}(\psi_{i+1,j+1} - \psi_{i-1,j+1}) \quad (46)$$

There are $N - 1$ equations of the form of Equation (41) and an equivalent number similar to Equation (42) for each grid line perpendicular to the direction of flow (for each value of the subscript $j + 1$).

The solution of this parabolic flow problem can be obtained from Equations (41) and (42) by solving the $N - 1$ equations for the stream function and the $N - 1$ equations for the vorticity for each row and then proceeding to the next row. Ordinarily, for a marching type of problem, there is no need to utilize an iterative technique in the numerical solution. However, since Equations (41) and (42) are coupled nonlinearly and since vorticity and stream function appear together in a boundary condition, the following numerical technique was used to proceed from the j^{th} row (where the vorticity and stream function distributions are known) to the $(j + 1)^{th}$ row:

1. Assume $N - 1$ values of the stream function and N values of the vorticity for the $(j + 1)^{th}$ row.
2. Compute new values of ψ for the $(j + 1)^{th}$ row by solving the $N - 1$ equations of the form of Equation (41) by tridiagonal matrix inversion.
3. Use the newly generated values of ψ and Equation (39) to evaluate a new value for $\omega_{N,j+1}$.
4. Compute new values of ω for the $(j + 1)^{th}$ row by solving the $N - 1$ equations of the form of Equation (42) by tridiagonal inversion of the square coefficient matrix.
5. Test ψ and ω for convergence of the iteration procedure.
6. If the convergence requirements are not met, repeat steps 2, 3, 4, and 5. If the convergence criteria are satisfied, proceed to the next axial step in the marching procedure.

With this computational scheme the solution is initiated at the tube entrance ($\zeta = 0$), where the flow field is known to be uniform, and is then marched down the tube. To obtain an accurate solution it was necessary to use a smaller axial increment near the tube entrance where abrupt changes in the flow development occur than elsewhere in the flow field. A solution was first obtained with $\Delta r = 0.05$ and $\Delta\zeta = 5 \times 10^{-4}$ for the first twenty steps and $\Delta\zeta = 5 \times 10^{-3}$ for all subsequent steps. The convergence of each step in the solution was determined by the same convergence test that was employed in the solution of the elliptic equations. The convergence of the finite-difference solution to the solution of the parabolic partial differential equations was verified by reproducing the results with a finer grid consisting of $\Delta r = 0.025$, $\Delta\zeta(j \leqq 80) = 1.25 \times 10^{-4}$, and $\Delta\zeta(j > 80) = 5 \times 10^{-3}$.

Axial and radial velocities were calculated from the finite-difference approximations to Equation (4) and to

$$N_{Re}V = \frac{1}{r}\frac{\partial\psi}{\partial\zeta} \quad (47)$$

Radial pressure gradients are everywhere zero under boundary-layer assumptions and axial pressure gradients were calculated from the finite-difference form of

$$\frac{N_{Re}}{2}V\frac{\partial U}{\partial r} + U\frac{\partial U}{\partial\zeta} = -\frac{1}{U_a^2\rho}\frac{\partial p}{\partial\zeta} + \frac{\partial^2 U}{\partial r^2} + \frac{1}{r}\frac{\partial U}{\partial r} \quad (48)$$

The total pressure drop was calculated from

$$\frac{\Delta p}{U_a^2\rho} = -2\left(\int_0^1 U^2\,r\,dr\right) + 1 - 2\int_0^\zeta (\omega)_{r=1}\,d\zeta \quad (49)$$

which was derived by integrating Equation (48) over the entire tube.

RESULTS AND DISCUSSION

The results of the numerical solution of the boundary-layer equations, as well as the analysis of the complete set of field equations at five different Reynolds numbers, are illustrated in Figures 1 to 9. Figures 1 and 2 show how the transfer of vorticity from the tube wall is influenced by the Reynolds number. At a Reynolds number of 250 (Figure 1) the convective transport of vorticity in the axial direction is much greater than the diffusive transport and very little vorticity is found in the upstream region. On the other hand, at very low Reynolds numbers such as illustrated in Figure 2, the diffusive mode of transport becomes relatively large and substantial quantities of vorticity appear in the stream tube region.

The development of the axial velocity fields for the different Reynolds numbers is illustrated in Figures 3 to 7. The velocity and vorticity fields are directly related;

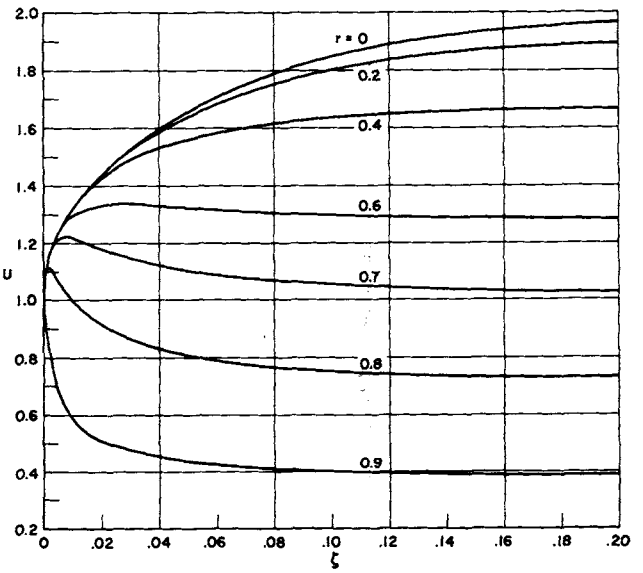

Fig. 8. Velocity distribution from boundary-layer equations.

TABLE 1. COMPARISON OF CASES STUDIED

Case	z_e	$2z_e/N_{Re}$	C
Boundary layer	—	0.225	1.18
$N_{Re} = 250$	26.75	0.214	1.28
$N_{Re} = 150$	14.38	0.192	1.36
$N_{Re} = 50$	4.70	0.188	1.40
$N_{Re} = 1$	0.66	1.32	7.76
$N_{Re} = 0$	0.62	—	—

therefore, the degree of velocity profile development that occurs upstream from the entrance increases as the Reynolds number is decreased. However, even when $N_{Re} = 0$ (the physically unrealizable flow situation of $N_{Re} = 0$ is meant to depict flow at very low Reynolds numbers, say, at $N_{Re} << 1$) substantial flow development occurs in the real tube. At this limit the velocity profile development in both regions is solely due to the diffusion of vorticity since the convective mode of transfer is ineffective. A comparison of Figure 7 with Figure 8 indicates that at $N_{Re} = 250$ the axial velocity distribution obtained from the solution of the complete field equations closely approximates the distribution obtained from the boundary-layer equations, the greatest deviation being near $z = 0$, the point where the boundary-layer assumptions are least applicable. Hence, at Reynolds numbers equal to or greater than 250, the boundary-layer equations adequately describe the flow field.

One interesting result that is not evident from the velocity distribution plots is that in some cases the velocity profile exhibits a concavity near the center of the tube. This effect was observed to be rather small with the maximum velocity never being more than 0.05% higher than the centerline velocity. Wang and Longwell (*13*) observed this same phenomenon in their numerical solution for flow between parallel plates, and Dealy (*4*) has discussed the importance of such an effect on the stability of flow. A much more pronounced effect was observed by Wang and Longwell when they used zero vorticity as a boundary condition at the entrance. However, such a boundary condition is artificial and unrealistic, since there is no way to stop the axial diffusion of vorticity at a particular point in the flow development. Like the analog involving the axial diffusion of a chemical species as discussed by Wehner and Wilhelm (*14*), the only realistic boundary condition is setting the value of the vorticity at some infinite limit.

The concavity in the velocity profile was not observed below a Reynolds number of 50 and the magnitude of this effect appears to increase with increasing Reynolds number. The trend with Reynolds number is weak and is not completely substantiated, since the concavities appear very close to the tube entrance in a region containing only a few grid points. However, it can be weakly inferred from these results that the concavity in the axial velocity profile increases with Reynolds number and may play a very important role in the stability of laminar flow in tubes.

The entrance length z_e, as shown in Figure 9 and Table 1, was defined as the dimensionless axial position at which the centerline velocity reached 99% of its fully developed value. It is evident that at the higher Reynolds numbers the axial diffusion of vorticity causes some velocity profile development upstream and, therefore, the entrance length is smaller than that predicted by the boundary-layer analysis. At very small Reynolds numbers the axial diffusion causes the velocity development to be spread downstream and the resulting entrance length is larger than that predicted by the boundary-layer analysis,

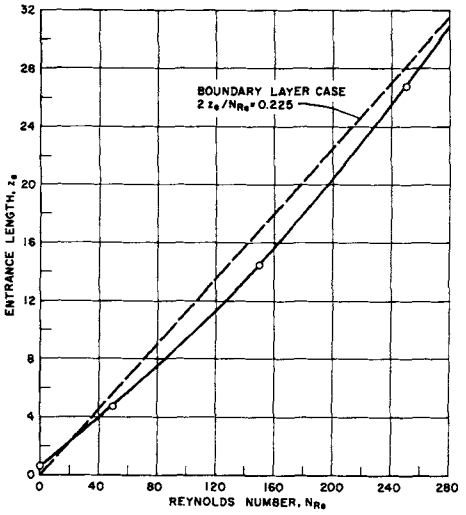

Fig. 9. Dependence of dimensionless entrance length on Reynolds number.

which considers only the convective transport of vorticity in the axial direction.

A total pressure drop was determined which is defined as the difference between the pressure at the one infinite limit of the stream tube and the pressure in the real tube where the flow becomes essentially fully developed. An excess pressure drop which is independent of radial position can then be defined as the difference between the total pressure drop and the pressure drop that would occur if the flow were uniform in all parts of the stream tube and fully developed in all parts of the real tube. Consequently, the dimensionless excess pressure drop C can be defined in the usual manner:

$$-\frac{\Delta p}{\frac{1}{2}U_a^2\rho} = \frac{32z}{N_{Re}} + C \qquad (50)$$

Table 1 shows that the dimensionless excess pressure drop increases with decreasing Reynolds number and is greater than that predicted by the solution of the boundary-layer equations.

Many investigators have analyzed the flow in the entrance of a tube by solving the boundary-layer equations. The results of several of these investigations are compared with the results of this study in Table 2. The investigations of Hornbeck (*6*) and Lemmon (*8*) involved the numerical solution of the boundary-layer equations in their conventional form, whereas the study of Campbell and Slattery (*2*) is the most recent of the more approximate methods which have utilized momentum integrals or a linearization of the equations of motion. The disagreement between the excess pressure drop obtained from the three numerical solutions may be due to the fact that different calculation schemes were used to determine the pressure distribution. On the other hand, there is excellent agreement between the velocity profiles obtained from the three different numerical solutions.

TABLE 2. COMPARISON OF BOUNDARY-LAYER SOLUTIONS

Investigator	$2z_e/N_{Re}$	C
This study	0.225	1.18
Hornbeck (*6*)	0.226	1.28
Lemmon (*8*)	0.222	1.275
Campbell and Slattery (*2*)	0.244	1.18

NOTATION

C = dimensionless excess pressure drop, defined by Equation (50)
e^{ijk} = three-dimensional permutation symbol
F_i = i^{th} component of external force per unit mass
g_{ij} = metric tensor
g^{ij} = associated metric tensor
g = determinant of metric tensor
k = numerical expansion parameter
k_r = expansion parameter for real tube
k_s = expansion parameter for stream tube
N_{Re} = Reynolds number $= 2R\,U_a\rho/\mu$
p = pressure
Δp = total pressure drop
R = radius of tube
r = radial distance/radius of tube
Δr = radial finite-difference increment
T_{ij} = stress tensor
t = time
U = axial component of velocity/average velocity in tube
U_a = average velocity in tube
V = radial component of velocity/average velocity in tube
v_i = covariant component of velocity vector
v^i = contravariant component of velocity vector
z = axial distance/radius of tube
z_e = dimensionless entrance length

Greek Letters

ϵ^{ijk} = $e^{ijk}/\sqrt{g}$
ζ = coordinate variable defined by Equation (24)
$\Delta\zeta$ = finite-difference increment for ζ
η = coordinate variable defined by Equation (16)
$\Delta\eta$ = finite-difference increment for η
μ = viscosity
ρ = density
ψ = dimensionless stream function
ω = dimensionless azimuthal physical component of vorticity vector
ω^i = i^{th} component of vorticity vector

LITERATURE CITED

1. Bird, R. B., W. E. Stewart, and E. N. Lightfoot, "Transport Phenomena," p. 45, Wiley, New York (1960).
2. Campbell, W. D., and J. C. Slattery, *Trans. Am. Soc. Mech. Engrs.*, **D85**, 41 (1963).
3. Carnahan, B., H. A. Luther, and J. O. Wilkes, "Applied Numerical Methods," p. 509 ff, Wiley, New York (1964).
4. Dealy, J. M., *A.I.Ch.E. J.*, **11**, 745 (1965).
5. Forsythe, G. E., and W. R. Wasow, "Finite-Difference Methods for Partial Differential Equations," p. 266 ff., Wiley, New York (1964).
6. Hornbeck, R. W., *Appl. Sci. Res.*, **A13**, 224 (1964).
7. Jones, C. W., and E. J. Watson, "Laminar Boundary Layers," L. Rosenhead, ed., p. 198 ff., Oxford Press, London (1963).
8. Lemmon, H. E., Ph.D. thesis, Univ. Utah, Salt Lake City (1963).
9. Lighthill, M. J., "Laminar Boundary Layers," L. Rosenhead, ed., p. 46 ff., Oxford Press, London (1963).
10. Morse, P. M., and H. Feshbach, "Methods of Theoretical Physics," p. 676 ff., McGraw-Hill, New York (1953).
11. Paris, Jean, and Stephen Whitaker, *A.I.Ch.E. J.*, **11**, 1033 (1965).
12. Truesdell, C., and R. A. Toupin, in "Handbuch der Physik," S. Flügge, ed., Band III/1, p. 353 ff., Springer, Berlin (1960).
13. Wang, Y. L., and P. A. Longwell, *A.I.Ch.E. J.*, **10**, 323 (1964).
14. Wehner, J. F., and R. H. Wilhelm, *Chem. Eng. Sci.*, **6**, 89 (1956).
15. Whitham, G. B., "Laminar Boundary Layers," L. Rosenhead, ed., p. 122, Oxford Press, London (1963).

APPENDIX

Vorticity Transport Equation in Curvilinear Coordinates

The covariant form of the equations of motion in curvilinear coordinates is

$$\rho\frac{\partial v_i}{\partial t} + \rho v^j v_{i,j} = \rho F_i + g^{jk}T_{ij,k} \qquad (A1)$$

and the stress tensor for an incompressible, Newtonian fluid can be written as

$$T_{ij} = -pg_{ij} + \mu(v_{i,j} + v_{j,i}) \qquad (A2)$$

In these equations, a comma denotes covariant differentiation and the usual summation convention is employed throughout. Substitution of Equation (A2) into Equation (A1) gives

$$\rho\frac{\partial v_i}{\partial t} + \rho v^j v_{i,j} = -\rho\phi_{,i} - p_{,i} + \mu g^{jk}v_{i,jk} \qquad (A3)$$

where it has been assumed that the external force field is conservative so that the external force can be expressed as the gradient of a potential:

$$F_i = -\phi_{,i} \qquad (A4)$$

By taking the curl of Equation (A3), we arrive at

$$\rho\frac{\partial(\epsilon^{nmi}v_{i,m})}{\partial t} + \rho\epsilon^{nmi}v^j{}_{,m}v_{i,j} + \rho\epsilon^{nmi}v^j v_{i,jm} = -\rho\epsilon^{nmi}\phi_{,im} - \epsilon^{nmi}p_{,im} + \mu\epsilon^{nmi}g^{jk}v_{i,jkm} \qquad (A5)$$

Since

$$\omega^n = \epsilon^{nmi}v_{i,m} \qquad (A6)$$

$$\epsilon^{nmi}v^j{}_{,m}v_{i,j} = -\omega^m v^n{}_{,m} \qquad (A7)$$

and since the curl of the gradient of a scalar is identically zero, Equation (A5) reduces to the vorticity transport equation in curvilinear coordinates:

$$\rho\frac{\partial\omega^n}{\partial t} + \rho v^j\omega^n{}_{,j} - \rho\omega^m v^n{}_{,m} = \mu\, g^{jk}\omega^n{}_{,jk} \qquad (A8)$$

The first two terms on the left represent the unsteady change and the convective transport of vorticity, whereas the term on the right side of Equation (A8) depicts the diffusive transport of vorticity. The third term on the left can be interpreted physically (*15*) as vorticity generation due to the deformation of the vortex tubes.

For the case of interest here, the body forces are prescribed so that the azimuthal velocity is zero and the axial and radial velocities are functions only of r and z. Hence, it follows from Equation (A6) that the components of the vorticity vector are

$$\omega^r = 0 \qquad \omega^z = 0 \qquad (A9)$$

$$\omega^\theta = \frac{1}{r}\left(\frac{\partial v_r}{\partial z} - \frac{\partial v_z}{\partial r}\right) \qquad (A10)$$

Therefore, the only component of the vector vorticity transport equation which remains is the azimuthal component, which takes the following form at steady state:

$$\rho(v^r\omega^\theta{}_{,r} + v^z\omega^\theta{}_{,z} - v^\theta{}_{,\theta}\omega^\theta) = \mu\left(\omega^\theta{}_{,rr} + \frac{\omega^\theta{}_{,\theta\theta}}{r^2} + \omega^\theta{}_{,zz}\right) \qquad (A11)$$

Evaluation of the covariant derivatives in Equation (A11) gives

$$\rho\left(v^r\frac{\partial\omega^\theta}{\partial r} + \frac{v^r\omega^\theta}{r} + v^z\frac{\partial\omega^\theta}{\partial z}\right) - \frac{\rho v^r\omega^\theta}{r} = \mu\left(\frac{\partial^2\omega^\theta}{\partial r^2} + \frac{3}{r}\frac{\partial\omega^\theta}{\partial r} + \frac{\partial^2\omega^\theta}{\partial z^2}\right) \qquad (A12)$$

where the convective transport terms have been separated from the term that represents the stretching of the vortex lines. Introduction of dimensionless variables and vector physical components into Equations (A10) and (A12) leads to Equations (7) and (8).

Manuscript received December 6, 1965; revision received March 3, 1966; paper accepted March 7, 1966.